Front. Optoelectron. 2013, 6(3): 251–260
DOI 10.1007/s12200-013-0358-2

RESEARCH ARTICLE

Investigation on layover imaging in synthetic aperture ladar

Zhaosheng YANG[1], Jin WU (✉)[2], Zhilong ZHAO[1], Donglei WANG[2], Yuanyuan SU[1], Na LIANG[1]

1 University of Chinese Academy of Sciences, Beijing 100039, China
2 Institute of Electronics, Chinese Academy of Sciences, Beijing 100190, China

Abstract Due to the short laser wavelength, almost all practical targets are rough. Surface elevations in rough targets will result in layovers in synthetic aperture ladar (SAL). High resolution SAL image with layovers will be different from the target picture taken by incoherent tools as digital camera. To investigate the layovers in SAL image, a simplified mathematical model is built by optics diffraction theory and a laboratory SAL is setup using 1550 nm tunable laser source. Layovers in SAL images, in both theoretical simulation and experimental demonstration, are carefully observed. Detailed results on various targets are illustrated.

Keywords synthetic aperture ladar (SAL), rough target, layover, simulation, demonstration

1 Introduction

As an optical analog of synthetic aperture radar (SAR), synthetic aperture ladar (SAL) could achieve ultrahigh resolutions in the long range with relative short synthetic aperture time [1]. Despite enormous difficulties in maintaining stable phase history data (PHD) during the synthetic aperture time due to the short optical wavelength, significant progress has been made on SAL development in the recent years [1–14].

SAL is usually a two-dimensional active imaging method with side-looking illumination, where target points with equal distance are placed in the same range element in the final focused SAL image. This is referred to as layover imaging in SAL. Up to now, most SAL imaging demonstrations are fulfilled using plane targets [1–11] and little attention is paid to the layover phenomenon. In fact, as SAL is applied to natural landscapes, layovers in the final focused images will probably be very common. In this sense, layover imaging investigation may be helpful to understand further details in the SAL image.

In this paper, layover imaging in SAL is specially addressed using optics terminology. By scalar diffraction theory, SAL imaging equations are setup and layover images of various targets are simulated. Using 1550 nm tunable laser source, high resolution SAL images with layovers are experimentally demonstrated.

Received June 18, 2013; accepted July 23, 2013

E-mail: jwu909@263.net

2 Mathematical simulation

2.1 Target model

In view of the optical wavelength used in SAL, all practical targets are rough targets. The surface fluctuations of the target can be approximately modeled as that in Ref. [15], where the target is simply considered to be composed of small planes vertically facing the SAL illuminating light beam with constant reflectivity and the varied heights of the platelets refer to the fluctuation of the surface roughness or elevation of the target. Mathematically, the surface reflectivity of a 3D target for SAL imaging can be approximated in 2D form by the following equation.

$$T(x_0,y_0,z_0) \approx \sum_{p,q} T(x_p,y_q)\delta(x_0-x_p)\delta(y_0-y_q), \quad (1)$$

where, $T(x_0,y_0,z_0)$ refers to the amplitude reflectivity at point (x_0,y_0,z_0) in the target coordinates as shown in Fig. 1; $T(x_p,y_q)$ is the amplitude reflectivity at target point (x_p,y_q) in the 2D target coordinate $(X_0O_0Y_0)$, and the summation is over all the target points.

2.2 SAL imaging equation

As given in Refs. [16,17], for rough targets with surface elevation, the SAL illumination geometry can be coordinated as in Fig. 1. We assume that the monostatic SAL adopts a rectangular aperture of sizes $D_x \times D_y$ for transmitting or receiving (T/R) laser pulses. Within one aperture synthesizing cycle, the main coordinate (XYZ) is

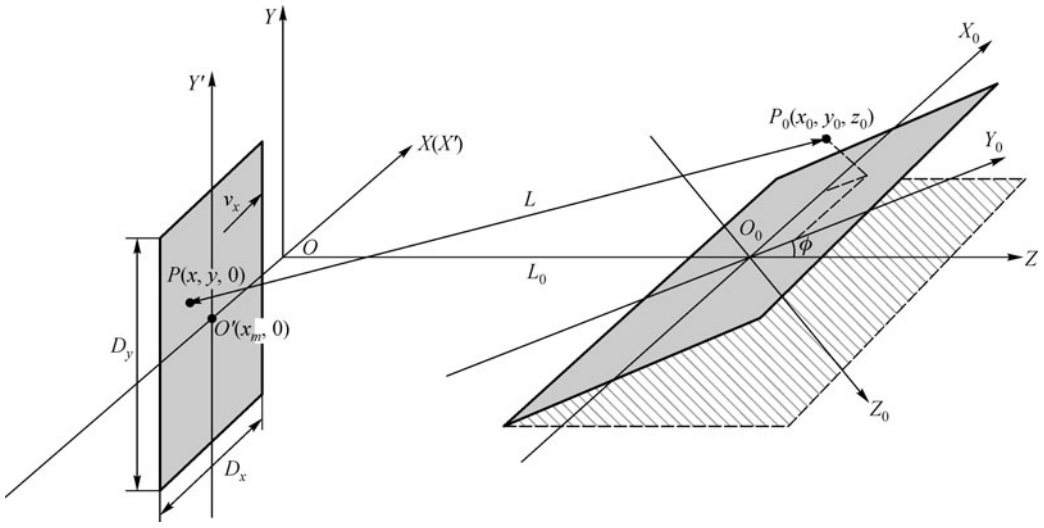

Fig. 1 Geometry of a sidelooking strip map mode SAL

fixed with its origin O at the aperture phase center and Z axis through the origin O_0 of the image plane ($X_0O_0Y_0$). The target coordinate ($X_0Y_0Z_0$) is set with X_0 axis parallel to the X axis in the main coordinate and Y_0 axis tilted with a angle ϕ to the Z axis in the main coordinate. The SAL coordinate is set as ($X'O'Y'$) with origin O' at the center of the T/R aperture and X' axis on the X axis in the main coordinate. The SAL is set moving along the X axis with constant velocity V_x.

In a strip-map mode SAL, the transmitted beam spot continuously sweeps across the target surface. As the SAL is positioned at $(x_m,0,0)$, by using scalar diffraction theory, the heterodyne signal, denoted as $R(x_m,t)$, for a strip-map mode SAL using quasi-chromatic linear chirped laser pulse illumination can be approximated as follows [16,17]:

$$R(x_m,t) = A\iint \mathrm{d}x_0\mathrm{d}y_0 \exp\left\{-\mathrm{j}\left\{2\pi f_0\left[t_0-\frac{2L_0}{c}-\frac{(x_m-x_0)^2+y_0^2+z_0^2+2L_0(y_0\cos\phi+z_0\sin\phi)}{cL_0}\right]\right.\right.$$

$$\left.\left.+\pi k\left[2t-t_0-\frac{2L_0}{c}-\frac{2(y_0\cos\phi+z_0\sin\phi)}{c}\right]\left[t_0-\frac{2L_0}{c}-\frac{2(y_0\cos\phi+z_0\sin\phi)}{c}\right]\right\}\right\} T(x_0,y_0,z_0)$$

$$\sin c^2\left(\frac{D_x}{\lambda_0}\frac{x_m-x_0}{L_0}\right)\sin c^2\left(\frac{D_y}{\lambda_0}\frac{y_0\sin\phi-z_0\cos\phi}{L_0}\right), \tag{2}$$

where, A covers all the constants that do not affect SAL imaging processing; f_0 is the baseline frequency of the transmitting light; t_0 is the delay time of the local light; c is the speed of light; L_0 is the target distance; k is the chirp rate; λ_0 is the laser wavelength that equals to c/f_0; D_x and D_y are the sizes of the rectangular T/R aperture respectively; and (x_0,y_0,z_0) refers to the target point $P_0(x_0,y_0,z_0)$ in the target coordinates; respectively.

With Eq. (2), the SAL image can be straightforwardly formed by using Fourier transformation with respect to time t and matched filtering with respect to x_m. The matched filter for azimuth focusing is expressed as follows

$$h(x_m) = \exp\left[-\mathrm{j}2\pi f_0\left(\frac{x_m^2}{cL_0}\right)\right]. \tag{3}$$

From Eq. (2), we can see that the roughness of the target surface will bring about phase shift in time domain, yielding frequency shift (so-called layover) after Fourier transform.

2.3 Simulation results

Using Eq. (2) and SAL parameters set in Table 1, we can simulate SAL images of targets with various surface fluctuations.

Table 1 SAL simulation parameters

parameter	value
baseline frequency f_0/Hz	1.9355e + 14
laser wavelength λ_0/nm	1550
chirp rate k/(Hz·s^{-1})	1.2490e + 13
pulse length/ms	170
T/R aperture $D_x \times D_y$/(μm×μm)	300 × 300
target distance L_0/m	2.4
azimuth step length/μm	50
synthetic aperture length/mm	8
SAL imaging mode	Stripmap
side-look angle ϕ	$\frac{\pi}{4}$

Theoretically, the SAL in Table 1 has an azimuth resolution of $\delta x_0 \approx 233$ μm and a range resolution of $\delta y_0 \approx 100$ μm.

Figure 2 simulates the SAL imaging of a big rectangular plate covered with a small rectangular plate. Figure 2(a) is the target setting showing two rectangular plates with height difference of 1 mm. Figure 2(b) shows the amplitude distribution of the raw SAL data. Figures 2(c) and 2(d) are the range compressed image and the azimuth focused SAL image, respectively. Figure 2(e) is the typical azimuth PHD in Fig. 2(c). From the final SAL image in Fig. 2(d), it can be seem that due to the height difference between the two planes, the small rectangular plate appears in a new range position and a vacancy is formed in the place where it actually sits. This is so called layover imaging in SAL.

Figure 3 is another simulated SAL image of a more complicated target. Figure 3(a) depicts the target setting, which is composed of four rectangular plates of the same size but different surface heights (the two short ones are of 50 μm, the front high one is of 250 μm and the highest is of 500 μm) . Figure 3(b) is the amplitude distribution of the raw SAL data. Figures 3(c) and 3(d) are the range compressed image and the final azimuth focused SAL image, respectively. Figure 3(e) shows the typical azimuth PHD in Fig. 3(c). From Fig. 3(d), apparent layovers induced by target surface elevations are displayed.

Figure 4 is the simulated SAL image of a rectangular rough target. Figure 4(a) shows the target setting, where both the surface reflectivity and surface height are set random. Figure 4(b) is the amplitude distribution of the raw SAL data, showing a chaotic interference pattern. Figures 4(c) and 4(d) are the range compressed image and the final azimuth focused SAL image, respectively. Figure 4(e) is the typical azimuth PHD in Fig. 4(c). Despite the layovers in SAL image formation, the rectangular shape of the target is kept in the final SAL image in Fig. 4(d).

From Figs. 2 to 4, SAL images on three types of targets are simulated. Depending on the target configuration in the SAL illuminating footprint, layovers in the SAL image can be clearly seen (Fig. 2), roughly seen (Fig. 3), or hardly seen (Fig. 4).

3 Experimental demonstration

3.1 Parameters of experimental SAL setup

The experimental parameters of the SAL setup are listed in Table 2.

Table 2 SAL experimental parameters

parameter	value
laser wavelength/nm	1550
target distance/m	2.4
wavelength scanning speed/(nm·s^{-1})	100
pulse length/ms	100
laser power/mW	5.0
SAL imaging mode	Stripmap/side-looking
azimuth step length/μm	50
synthetic aperture length/mm	8

From Table 2, the theoretical estimation of the resolutions in the SAL setup can be calculated out as:

Range resolution: $\delta y_0 \approx 170$ μm (45° side-looking);

Azimuth resolution: $\delta x_0 \approx 233$ μm.

3.2 Experimental results

Figure 5 shows the results of a small rectangular plate on a big rectangular plate with height difference of about 2.5 mm. The target is made of "3M" diamond retro-reflecting materials. Figure 5(a) is the photograph of the target plate. Figure 5(b) shows the amplitude distribution of the raw SAL data. Figures 5(c) and 5(d) are the range compressed image and azimuth focused SAL image, respectively. Figure 5(e) is the black/white pattern of Fig. 5(d). Apparent layover could be found from Figs. 5(d) and 5(e). Figure 5(f) is the azimuth PHD in Fig. 5(c). And as predicted in Fig. 2, a vacancy is formed in Fig. 5(d) due to the layover imaging.

Figure 6 shows the result of a target composed of four small rectangular planes with different heights. Figure 6(a) shows the photograph of the target, where the left two rectangle plates are one layer high of about 0.42 mm, the lower right one is two layer high of about 0.84 mm and the upper right one is four layer high of about 1.68 mm. Figure 6(b) is the raw SAL data. Figures 6(c) and 6(d) are the range compressed image and azimuth focused image, respectively. Figure 6(e) is the typical azimuth PHD in Fig. 6(c). The layovers shown in Fig. 6(d) are almost the same as that simulated in Fig. 3.

Figure 7 shows the result of a rough target. The target is

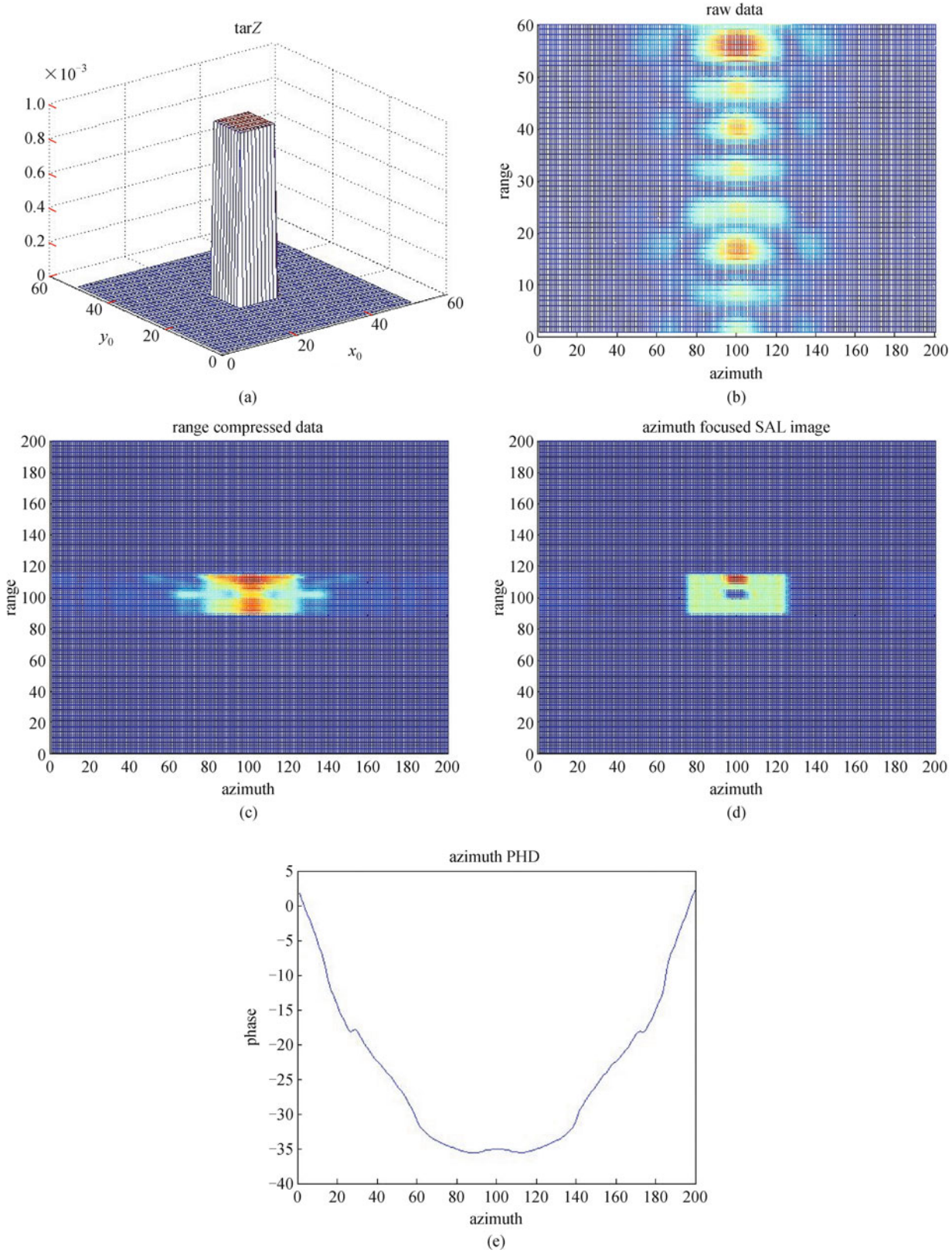

Fig. 2 SAL image simulation of a small rectangular plate on a big rectangular plate. (a) Target setting; (b) raw SAL data; (c) range compressed image; (d) azimuth focused image; (e) azimuth PHD

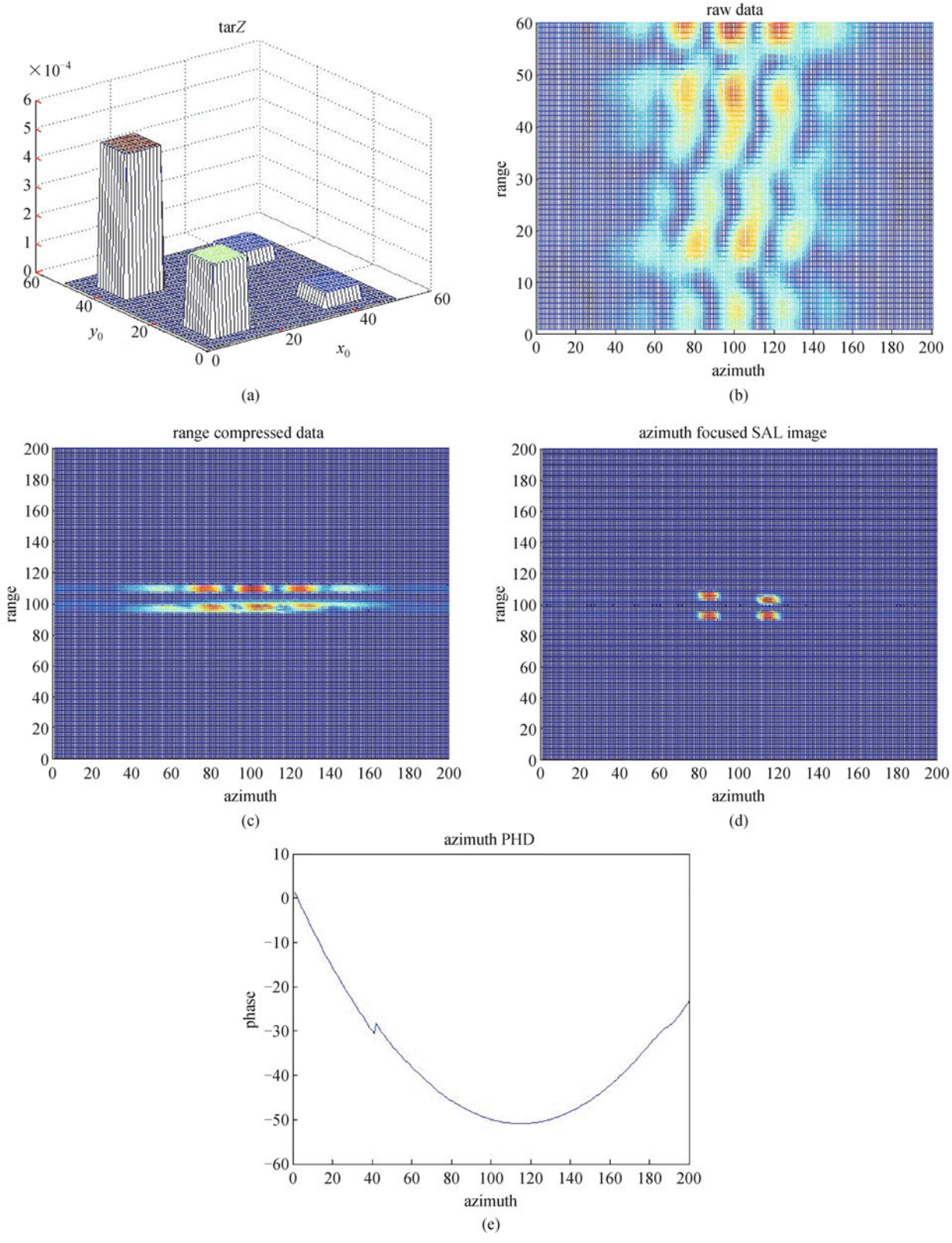

Fig. 3 SAL image simulation of a four-rectangular-plate target. (a) Target setting; (b) raw SAL data; (c) range compressed image; (d) azimuth focused image; (e) azimuth PHD

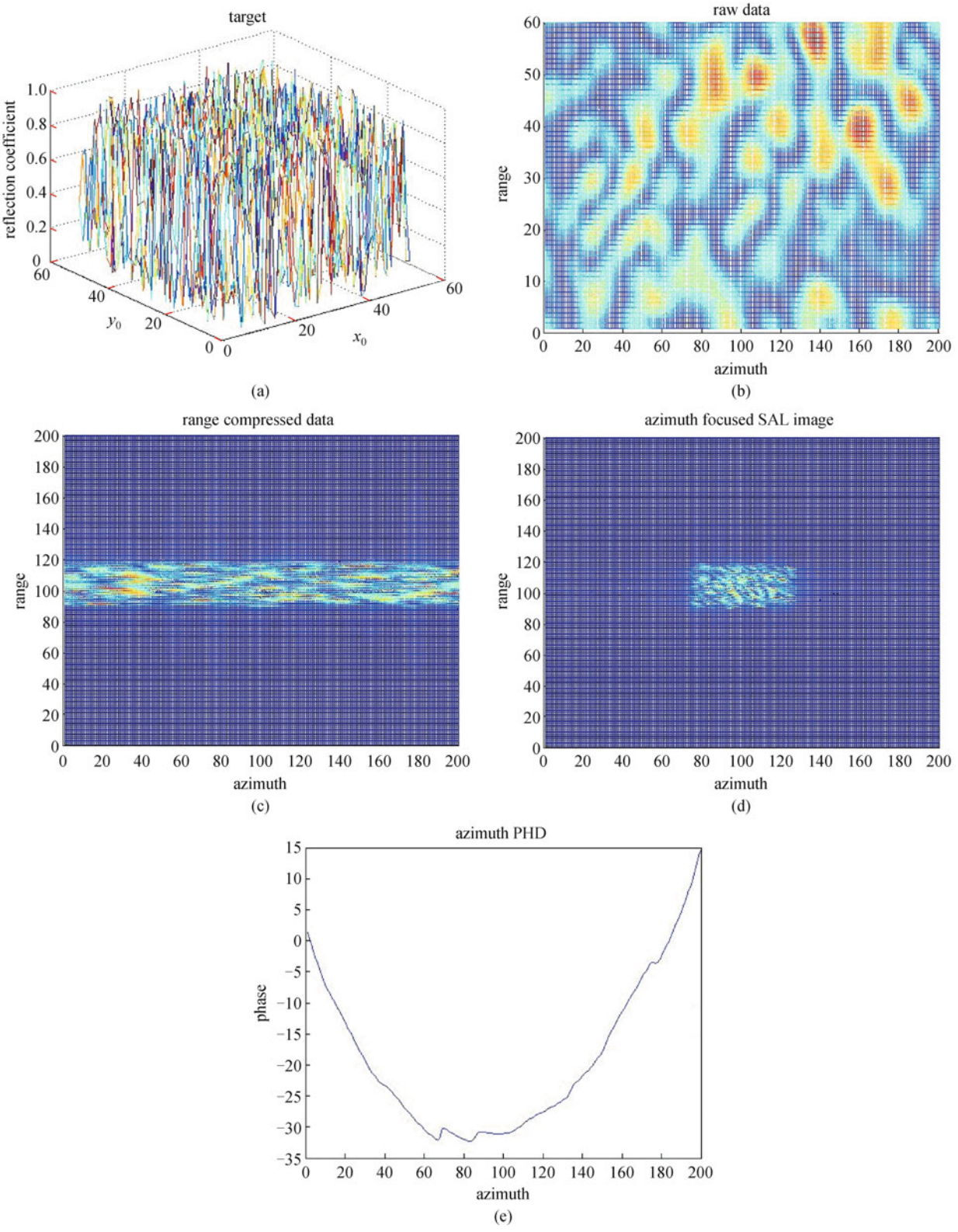

Fig. 4 SAL image simulation of a rectangular rough target. (a) Target setting; (b) raw SAL data; (c) range compressed image; (d) azimuth focused image; (e) azimuth PHD

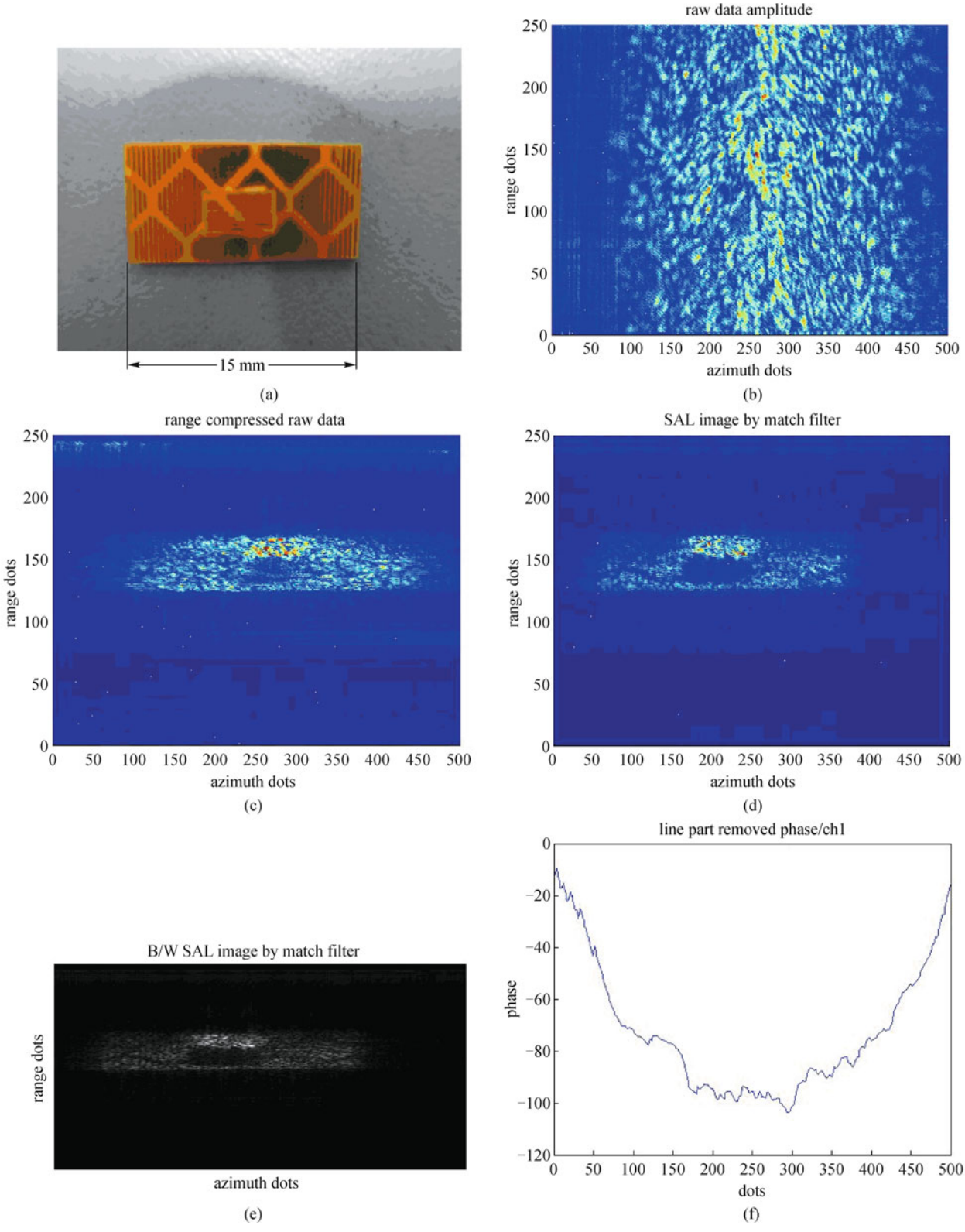

Fig. 5 SAL images of a small rectangular plate on a big rectangular plate. (a) Photograph of the target; (b) raw SAL data; (c) range compressed image; (d) azimuth focused SAL image; (e) black/white (B/W) SAL image; (f) azimuth PHD

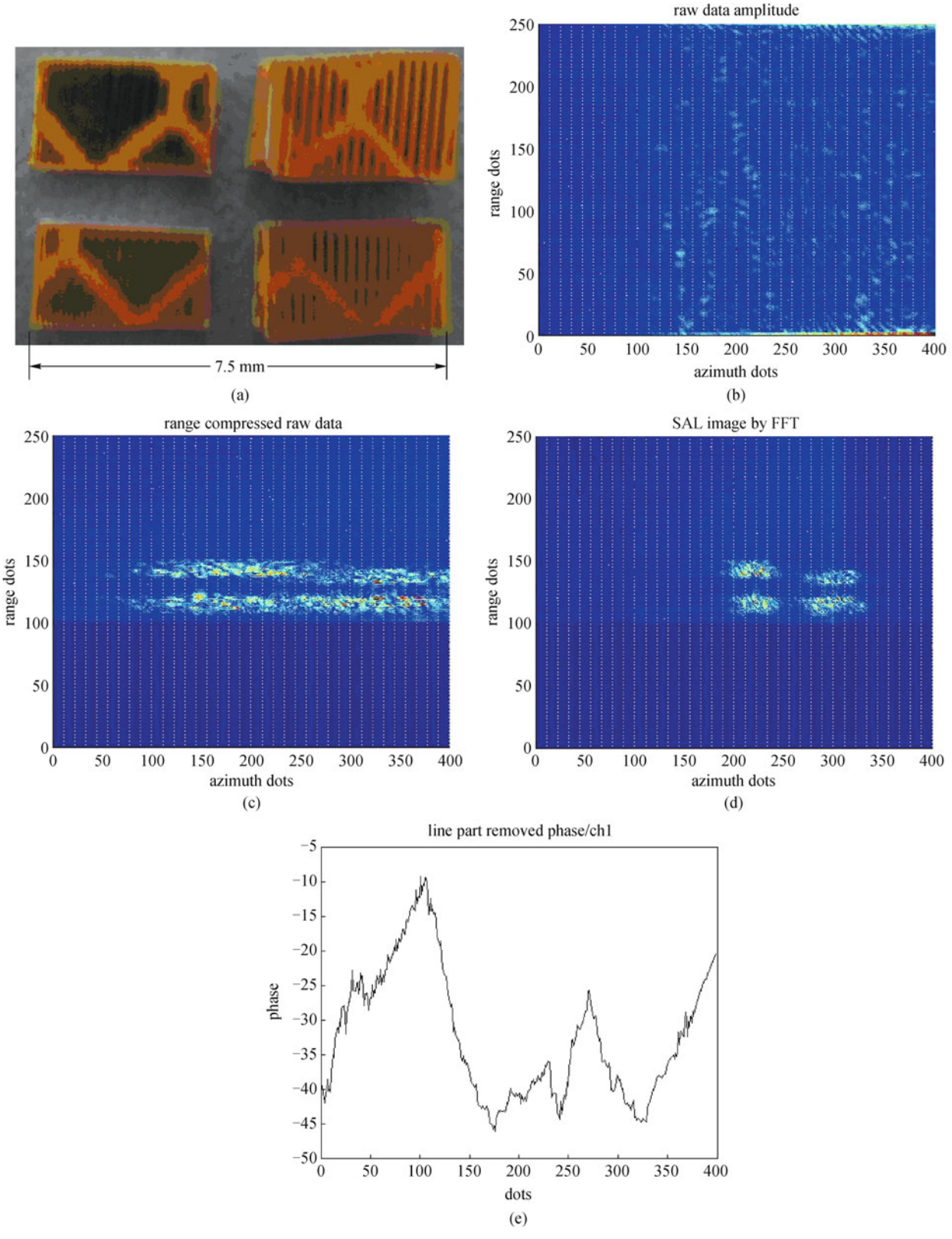

Fig. 6 SAL images of four rectangular plates. (a) Photograph of the target; (b) raw SAL data; (c) range compressed image; (d) azimuth focused SAL image; (e) azimuth PHD

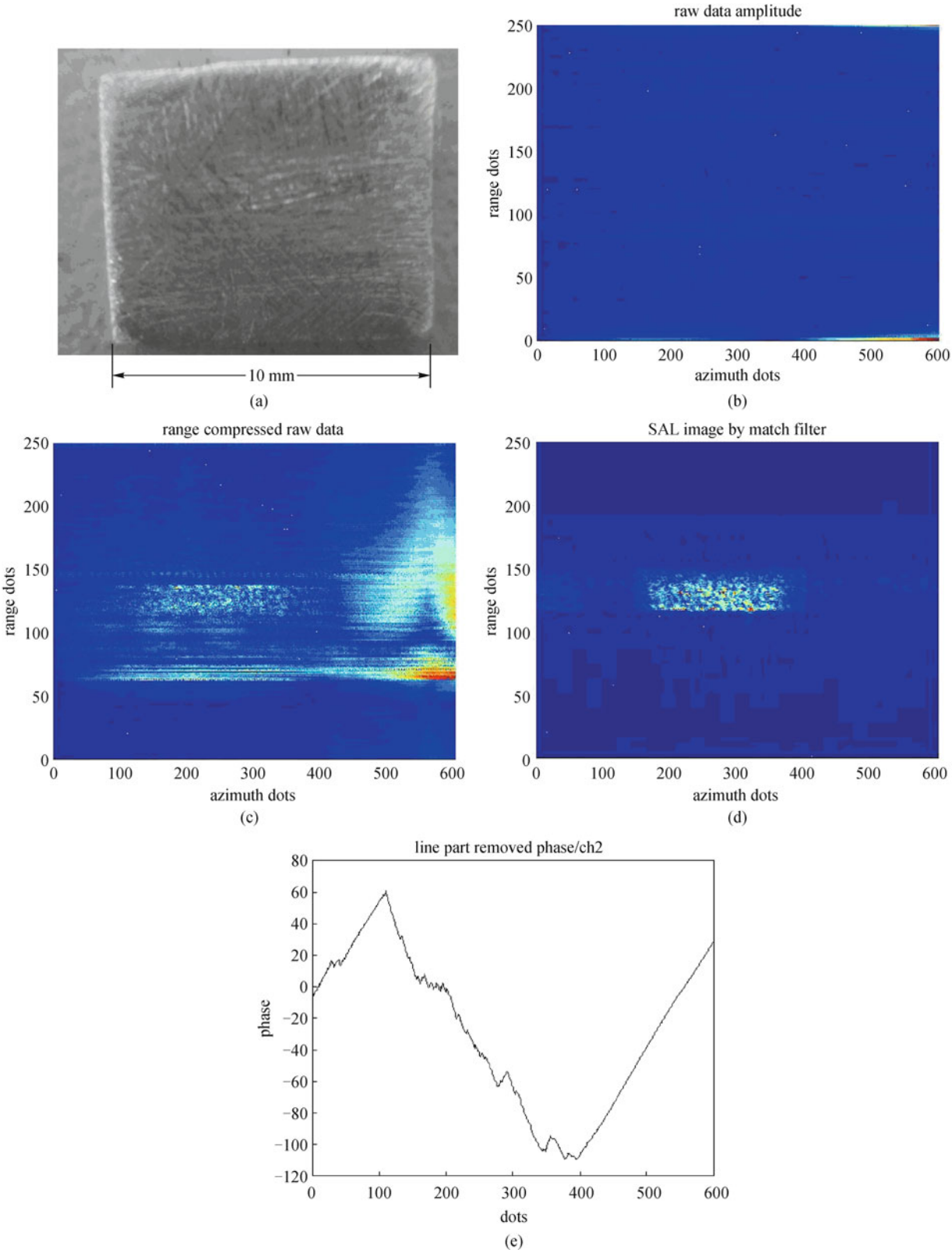

Fig. 7 SAL images of a randomly polished aluminum plate. (a) Photograph of the aluminum foil; (b) raw SAL data; (c) range compressed image; (d) azimuth focused SAL image; (e) azimuth PHD

made of aluminum foil with its surface randomly polished by fine sand paper. Figure 7(a) is the photograph of the 10 mm×10 mm size foil. Figure 7(b) is the raw SAL data. Figure 7(c) is the amplitude distributions of the range compressed image and Fig. 7(d) is the azimuth focused SAL image. Figure 7(e) is the typical azimuth PHD in Fig. 7(c). From Figs. 7(b) to 7(d), a typical two-step focusing is displayed. Due to the poor backscattering of the rough aluminum surface, very dimly interference pattern is shown in the raw data in Fig. 7(b). A well focused rectangular pattern is formed after range compression and azimuth synthetic aperture processing.

4 Conclusions

Layover imaging in SAL is investigated both mathematically and experimentally. The mathematical simulation is fulfilled by optics diffraction and the experimental demonstration is using 1550 nm wavelength tunable laser source. Detailed imaging results together with their azimuth PHD on typical targets are illustrated. Layover images observed in the experimental demonstration are in good agreement with those in the mathematical simulation.

Due to the short optical wavelength and high resolution, layover imaging in SAL will be much more common than that in SAR. As we demonstrated, for certain simple targets, there will be apparent vacancy in the final SAL image; however, for those complicated targets, layovers in the SAL image are hardly seen.

Despite SAL flight test has been demonstrated [5], SAL images, especially those on practical targets, are still far from sufficient in the scientific literatures for further study. Detailed results, either in laboratory or on practical moving platforms, are still welcomed in SAL development.

Acknowledgements This work, initially sponsored by the National High Technology Research and Development Program of China (863 Program) (No. 2007AA12Z107) in 2007, is currently funded by National Natural Science Foundation of China (Grant No. 61178071). We greatly appreciate the help on SAR signal processing by vice Prof. Chang Liu in the Institute of Electronics, Chinese Academy of Sciences.

References

1. Bashkansky M, Lucke R L, Funk E E, Reintjes J F, Rickard L J. Synthetic aperture imaging at 1.5 μm: laboratory demonstration and potential application to planet surface studies. Proceedings of the Society for Photo-Instrumentation Engineers, 2002, 4849: 48–56
2. Bashkansky M, Lucke R L, Funk E, Rickard L J, Reintjes J. Two-dimensional synthetic aperture imaging in the optical domain. Optics Letters, 2002, 27(22): 1983–1985
3. Beck S M, Buck J R, Buell W F, Dickinson R P, Kozlowski D A, Marechal N J, Wright T J. Synthetic-aperture imaging laser radar: laboratory demonstration and signal processing. Applied Optics, 2005, 44(35): 7621–7629
4. Buck J R, Krause B W, Malm A I R, Ryan C M. Synthetic aperture imaging at optical wavelengths. In: Proceedings of International Quantum Electronics Conference. Optical Society of America, 2009
5. Krause B, Buck J, Ryan C, Hwang D, Kondratko P, Malm A, Gleason A, Ashby S. Synthetic aperture ladar flight demonstration. In: Proceedings of CLEO: Science and Innovations. Optical Society of America, 2011
6. Zhou Y, Xu N, Luan Z, Yan A M, Wang L J, Sun J F, Liu L R. 2D imaging experiment of a 2D target in a laboratory–scale synthetic aperture imaging ladar. Acta Optica Sinica, 2009, 29(7): 2030–2032 (in Chinese)
7. Liu L R, Zhou Y, Zhi Y N, Sun J F, Wu Y P, Luan Z, Yan A M, Wang L J, Dai E W, Lu W. A large aperture synthetic aperture imaging ladar demonstrator and its verification in laboratory space. Acta Optica Sinica, 2011, 31(9): 0900112 (in Chinese)
8. Dai E W, Sun J F, Yan A M, Zhi Y N, Zhou Y, Wu Y P, Liu L R. Demonstration of a laboratory Fresnel telescope synthetic aperture imaging ladar. Acta Optica Sinica, 2012, 32(5): 0528003 (in Chinese)
9. Buell W F, Marechal N J, Buck J R. Synthetic-aperture imaging ladar. Aerospace Corporation Magazine of Advanced Technology, 2004, 5(2): 45–49
10. Dierking M, Schumm B, Ricklin J C, Tomlinson P G, Fuhrer S D. Synthetic aperture LADAR for tactical imaging overview. In: Proceedings of 14th Coherent Laser Radar Conference (CLRC), 2007, 191–194
11. Guo L, Xing M D, Zhang L, Tang Y, Bao Z. Research on indoor experimentation of range SAL imaging system. Science in China Series E: Technology Sciences, 2009, 52(10): 3098–3104
12. Hong G L, Wang J Y, Meng Z H, Li J W, Tong P, Shu R. Chirped amplitude modulation and range dimension processing of near infrared synthetic aperture ladar. Journal of Infrared and Millimeter Waves, 2009, 28(3): 229–234 (in Chinese)
13. Liu L R. Principle of down-looking synthetic aperture imaging ladar. Acta Optica Sinica, 2012, 32(9): 0928002 (in Chinese)
14. Crouch S, Barber Z W. Laboratory demonstrations of interferometric and spotlight synthetic aperture ladar techniques. Optics express, 2012, 20(22): 24237–24246
15. Tavassoly M T, Nahal A, Ebadi Z. Image formation in rough surfaces. Optics Communications, 2004, 238(4–6): 252–260
16. Wu J. Matched filter in synthetic aperture ladar imaging. Acta Optica Sinica, 2010, 30(7): 2123–2129 (in Chinese)
17. Zhao Z L, Wu J, Li F F, Yang Z S. Calculation and simulation on vibrating targets imaging in stripmap mode synthetic aperture ladar. Acta Optica Sinica, 2012, 32(8): 0828006 (in Chinese)